Theor Chem Acc (1999) 101:247–256
DOI 10.1007/s002149800m87

Theoretical
Chemistry Accounts

Regular article

Convergence of the density functional one-centre expansion for the molecular continuum: N_2 and $(CH_3)_3N$

M. Stener, G. De Alti, P. Decleva

Dipartimento di Scienze Chimiche, Università di Trieste, Via L. Giorgieri 1, I-34127 Trieste, Italy

Received: 19 May 1998 / Accepted: 20 August 1998 / Published online: 7 December 1998

Abstract. A large-scale one-centre expansion with a radial B-spline basis set is implemented for bound and continuum states. A Kohn-Sham hamiltonian is employed with Hartree and exchange-correlation potentials calculated from the SCF electron density taken from a previous LCAO calculation. An inverse iteration method is used to obtain the continuum wavefunction, from which the cross section and asymmetry parameter are calculated. The convergence with respect to angular momentum and cut-off radius is analysed for N_2. The relevance of multipolar contributions even at large distances is shown and suggestions for further improvements are given. In order to show that the present method is suitable to treat systems of moderate size, the $(CH_3)_3N$ molecule has also been calculated and the results are compared with experiment.

Key words: Density functional one-centre expansion – Molecular continuum – Nitrogen – Trimethylamine

1 Introduction

In recent years, a general growing and easier availability of new synchrotron radiation sources has generated more interest in the photoabsorpion and photoemission processes which can be much more easily studied with this technique than with conventional sources [1]. Such experimental data (i.e. the cross section and the asymmetry parameter) are closely connected with the electronic structure of the probed system. However, the rationalization of the measured data is not direct at all and therefore a relevant contribution to the discussion of the results may come from the theory.

On the other hand, such calculations need the explicit description of a molecular continuum wavefunction, which is still far being a standard approach in the field of quantum chemistry, unlike the bound states whose treatment is much better consolidated. Actually the only approach capable of obtaining full continuum wavefunctions for large polyatomic molecules is the old CMSM method [2]. However, it has proved hard to improve the drastic MT approximation which is known to be rather inaccurate. In practice, the MS method has been virtually abandoned for bound state calculations in favour of the much more accurate LCAO approach.

An interesting alternative is given by the Stieltjes imaging technique [3]: the cross section is extracted from a discrete pseudospectrum obtained with a conventional bound state approach, making the problem much simpler. However, this method has several limitations, for example sharp structures are missed or very poorly reproduced and the angular distribution cannot be obtained. Therefore it is apparent that only a method capable of treating explicitly the continuum will be able to furnish a complete and reliable answer in this field.

Despite several attempts [4–7], it is not yet clear which direction might lead to the best solution, although one may reasonably expect that a combination of a one-centre expansion (OCE), able to describe the oscillatory behaviour of the continuum wavefunction up to the asymptotic region, and a conventional LCAO set, like a bound state GTO basis to take care of the nuclear cusps, might be quite accurate.

It is apparent, however, that highly accurate and robust numerical algorithms must be employed, because of the numerical linear dependence associated with the large basis set and the highly excited nature of the continuum eigenvectors which give rise to delicate numerical instabilities.

Along this line, the development of a robust and accurate OCE approach is an essential step. Although the pure OCE approach is very slowly convergent for bound states, for the continuum, better performances may be expected, owing to the different shape of the wavefunction. An additional interest of the OCE approach is the ease with which matrix elements can be evaluated, which gives the opportunity of employing the full range of many-body approaches.

Correspondence to: M. Stener

In this work we analyse the performances of a new density functional – one centre expansion (DF-OCE) method, employing a B-spline finite radial basis set. The B-spline basis set has proven a very promising choice [8], owing to its high accuracy, the avoiding of numerical linear dependence and the flexibility in handling the boundary condition for the wavefunction or the potential. Within the OCE approach, a basis-set-free fully numerical method would have been, in principle, another possible choice. We have decided, anyway, to work with a finite basis set Galerkin method because we intend to extend the present approach to the molecular LCAO formulation. Nevertheless, a comparison between spline algorithms and traditional numerical methods [9] shows that the former perform, in general, better than the latter. Moreover, spline algorithms are more suitable to be implemented for modern computers, because the problem is recast to a linear algebraic one and therefore it can take advantage of highly optimized standard routines.

The present method employs a Kohn-Sham (KS) hamiltonian with local exchange-correlation potential, and therefore a single-determinant ansatz is assumed; nevertheless, the electron correlation is formally considered. The theoretical method might be improved by introducing the TDLDA formalism [10, 11], which should be straightforward in this OCE approach.

The present work is focused mainly on the convergence of the OCE approach rather than on the accuracy of the DF method. In fact it is well known that the OCE approach demands very high angular momentum to give stable results when heavy off-centre nuclei are present; for this reason the N_2 molecule has been chosen as a test case. The convergence has proven to be rather fast and regular in the present case. In order to show that the method is suitable to treat larger systems as well, it has been applied to trimethylamine $(CH_3)_3N$, giving convergent results which compare well with experiment.

2 Theoretical method

The salient features of the present method can be summarized accordingly to the following three points:

1. A general least-squares algorithm to compute continuum eigenvectors at any given photoelectron energy.
2. A choice of a local one-particle hamiltonian based on the LDA potential.
3. A choice of a one-centre B-spline basis set.

They will be discussed separately in the following.

2.1 Continuum states

Once a proper basis set is chosen, the overlap and hamiltonian matrix are evaluated:

$$S_{ij} = \langle \chi_i \chi_j \rangle, \qquad H_{ij} = \langle \chi_i, H\chi_j \rangle$$

A complete set of independent eigenvectors relative to a given photoelectron energy E is then obtained as eigenvectors of the non-hermitean, energy-dependent matrix $\mathbf{A}$:

$$\mathbf{A}(E)c = ac, \qquad \mathbf{A}(E) = \mathbf{H} - E\mathbf{S}$$

corresponding to minimum modulus eigenvalues. These eigenvectors, neatly separated from the others, are efficiently obtained by block inverse iteration [8], which recasts the problem to a linear system. For this fundamental task, highly optimized routines are available on most computers [12].

The continuum states $\varphi_n(\mathbf{r})$ are normalized accordingly to the $\mathbf{K}$ matrix asymptotic conditions, matching the asymptotic part of the non-normalized $\varphi'_n(\mathbf{r})$ eigenvectors with respect to the regular and irregular Coulomb wave functions [13]:

$$\varphi'_n(\mathbf{r}) \underset{\infty}{\to} \sum_{lm} [a_{lm,n} f_l(r) + b_{lm,n} g_l(r)] Y_{lm}(\vartheta, \varphi)$$

and the two matrices $\mathbf{A}$ and $\mathbf{B}$ are obtained. Since the transition state (TS) electron configuration is chosen (see Sect. 2.2), the charge of the Coulomb wavefunction is set to 1/2. The $\mathbf{K}$ matrix is defined as $\mathbf{K} = \mathbf{B}\mathbf{A}^{-1}$, and the continuum is normalized accordingly to:

$$\varphi_n(\mathbf{r}) \underset{\infty}{\to} \sum_{lm} [\delta_{lm,n} f_l(r) + K_{lm,n} g_l(r)] Y_{lm}(\vartheta, \varphi)$$

Dipole matrix elements in the length gauge are further transformed to $\boldsymbol{S}$-matrix representation, and the cross section and asymmetry parameter are computed within the formalism of the angular momentum transfer [14]. Owing to the local nature of the present hamiltonian, the velocity gauge results should not differ from the length form, apart an error due to the non-completeness of the basis set. However, the present basis is very extended so we can reasonably expect only very small differences.

The discrete spectrum is obtained by conventional diagonalization of the hamiltonian matrix. It is worth noting that the approach is very simple, so that its computational implementation can be done in a very efficient manner. The dipole transition moments are calculated between the continuum and the bound states, the latter being obtained by the same OCE approach.

2.2 One-particle hamiltonian

Since the main goal of the present work is to test the convergence and the performance of basis with respect to the continuum, we have chosen a single-particle hamiltonian based on a local potential. The present LDA has probably an accuracy similar to the commonly employed static-exchange approximation [15], and this limits the capability of the method with respect to the experiment. Actually, only a very few small molecules have been treated beyond the one-particle hamiltonian with an explicit continuum treatment, including N_2 [16] which will serve as a useful comparison with present study.

The hamiltonian presently employed is built from the electron density, accordingly to the Kohn-Sham scheme [17]:

$$h_{\mathrm{KS}} = T + V_{\mathrm{N}} + V_{\mathrm{C}} + V_{\mathrm{XC}}$$

where

$$V_{\mathrm{C}} = \int \frac{\rho(2)}{r_{12}} \mathrm{d}r_2, \qquad V_{\mathrm{XC}} = V_{\mathrm{XC}}[\rho(r)]$$

are the classical coulomb potential (Hartree) and the local approximation to the exchange-correlation potential, respectively.

The electron density ρ is obtained from a conventional bound state calculation with an LCAO scheme; then it is decomposed into its angular components (see following Sect. 2.3.) in order to build the OCE hamiltonian. The TS electron configuration is chosen, that is, half an electron is removed from the ionized orbital. This is a common practice in the CMSM method and has been corroborated by wide tests with different potentials [18]. A first attempt to analyse the consequences of the potential choice (electron configuration as well as exchange correlation) has been carried out [18], although that work was limited (in the molecular case) by the Stieltjes imaging technique employed to extract the cross-section profiles. Nevertheless, owing to the limited experience in this field, a further more precise analysis on the optimal potential choice may be desirable. Such an analysis may be profitably carried out with the present method, which should be sufficiently accurate for numerical solutions to give a reliable answer. It is important to

mention here that new exchange-correlation potentials with correct asymptotic behaviour [19] might improve the description of photoionization properties, as has been already observed for other properties like dynamic polarizability [20], which are very sensitive to the description of the electronic structure in regions far from the atomic nuclei.

2.3 B-spline basis set

The one-centre expansion consists [21, 22] in a basis set factorized in a radial function times a spherical harmonic on a common centre:

$$\chi_{nlm} = \frac{1}{r} B_n(r) Y_{lm}(\vartheta, \varphi)$$

The $B_n(r)$ radial basis set used consists of B-spline functions, over a given interval [0, $R_{\max}$]: they are piecewise polynomials defined according to their order k and to a grid of knots:

$$0 = t_0 \leq t_1 \leq \ldots \leq t_n = R_{\max}$$

B-spline functions have the remarkable property to be non-zero only over an interval spanned by consecutive $k+1$ knots (giving band sparse matrices), to have good numerical approximation properties and to be available in FORTRAN routines [23]. Moreover, they have been widely applied to atomic and molecular electronic structure calculations [24, 25]. In the one-centre basis, angular integrals are analytical, while radial integrals are efficiently evaluated with machine accuracy by Gauss-Legendre integration.

In order to take advantage of the symmetry, the basis is symmetrized with respect to the irreducible representations $\lambda\mu$ of the molecular point group [22]:

$$X_{lh\lambda\mu}(\vartheta, \varphi) = \sum_m Y^R_{lm}(\vartheta, \varphi) B_{lmh\lambda\mu}$$

The density and the potential are expanded in their angular components over the real spherical harmonics:

$$f(r, \vartheta, \varphi) = \sum_{l,m} R_{l,m}(r) Y^R_{l,m}(\vartheta, \varphi)$$

the $R_{l,m}(r)$ expansions being obtained by numerical integration over an angular grid (the direct product of two monodimensional Gauss-Legendre sets of points and weights):

$$R_{l,m}(r) = \iint f(r, \vartheta, \varphi) Y^R_{l,m}(\vartheta, \varphi) \sin\vartheta \, \mathrm{d}\vartheta \, \mathrm{d}\varphi$$

The radial components of the V_C potential are efficiently calculated from the Poisson equation in the same basis set:

$$\nabla^2 V_C = -4\pi\rho$$

The problem is so recast to an algebraic linear system, whose matrix is simply the Laplacian representation within the basis set, and the right-hand side is a vector whose elements are the integrals of the radial expansions with the basis functions. The solution of the linear system gives immediately the radial components of V_C. It must be considered that each angular momentum in V_C gives rise to specific boundary conditions for the potential:

$$\lim_{r\to\infty} V_{lm} = M_{lm}/r^{l+1}$$

where M_{lm} corresponds to the electric multipole. The B-spline functions are very flexible, so the boundary conditions are easily implemented, imposing a constraint to the logarithmic derivative at $R_{\max}$.

3 Computational details

3.1 N_2

The N_2 molecule has been considered with the experimental N-N distance of 2.068 a.u.; the centre of the expansion has been set in the centre of mass. A radial B-spline basis set of order 10 has been built on a radial linear grid, with a step size of 0.1034 a.u. and 200 intervals, the cut-off radius being 20.68 a.u. This choice for the step size has been dictated by the requirement to put one grid knot on the nuclei. The SCF electron density was previously calculated by means of the ADF program [26], with the VWN exchange-correlation potential [27] and with an extended STO basis set [28] supplemented with two $3d$ polarization functions with exponents 2.5 and 1.5.

Standard generalized diagonalization is used to obtain bound states, while LU decomposition is used to perform the inverse iteration procedure for the continuum.

In order to reduce significantly the dimensions of the problem, the full radial basis set is used only up to angular momentum $L = 9$, while for higher values only the first 20 B-splines have been used, since their contribution is important only in the vicinity of the nuclei.

The TS electron configuration is used during the SCF process, i.e. half an electron is removed from the orbital which is ionized. In each case the proper TS configuration has been chosen and the photon energy is calculated as the sum of the kinetic energy (KE) and the experimental threshold. For the core $1\sigma_g$ (N $1s$) state the reduced $C_{\infty v}$ symmetry is employed in order to allow the core hole localization.

3.2 $(CH_3)_3N$

The experimental geometry has been used for $(CH_3)_3N$ [29]; in this case the centre of expansion has been set on the intersection of the three-fold axis of the molecule with the plane defined by the nuclei of the three carbon atoms. The B-spline basis set is of order 10, over a grid of 101 intervals and a cut-off radius of 15.5 a.u. The step size is not constant near to the origin; it is slightly adapted in order to have a knot on the N and C nuclei; at distances $R \geq 2.75$ a.u. the step size is constant and equal to 0.15 a.u. The maximum angular momentum in the OCE has been kept fixed to $L_{\max} = 25$. The STO basis set for the SCF-LCAO calculation has been taken from [28] for C and N, supplemented with two $3d$ polarization functions with exponents 1.5 and 3.0 for C and with exponents 1.5 and 2.5 for N. For H, a $3s1p$ basis set has been used, with the following exponents: $\alpha_{1s} = 0.69$, 0.92 and 1.58; $\alpha_{2p} = 1.00$. For $(CH_3)_3N$, only the valence ionizations have been analysed, so the complete C_{3v} point group symmetry is always employed. All the other details are the same as for N_2.

4 Results and discussion

The principal aim of this work is to study the stability and the convergence of the present OCE algorithm, and to investigate convergence patterns with respect to the maximum angular momentum employed ($L_{\max}$), and the cut-off radius ($R_{\max}$). Moreover, since good performances have been obtained, we decided to apply the present method to the trimethylamine molecule. Owing to its large extension and moderate symmetry, it represents a challenging test for methods oriented to an accurate treatment of the electronic continuum.

4.1 N_2

The KS eigenvalues of N_2 have been calculated employing the transition state $(3\sigma_g)^{-1/2}$ configuration and $D_{\infty h}$ symmetry. The trend with respect to $L_{\max}$ is reported in Table 1, compared to the LCAO values obtained with the basis set described in Sect. 3, while full convergence is achieved already at the smallest $R_{\max}$ employed. The core levels $1\sigma_g$ and $1\sigma_u$ are very slowly convergent, the

Table 1. KS eigenvalues (a.u.) of N_2 calculated at different values of L_{max}; R_{max} kept fixed at 10.34 au

State	L_{max}				LCAO
	40	50	60	80	
$1\sigma_g$	−14.0285	−14.0928	−14.1196	−14.1363	−14.2742
$2\sigma_g$	−1.3363	−1.3397	−1.3410	−1.3419	−1.3431
$3\sigma_g$	−0.6619	−0.6624	−0.6626	−0.6628	−0.6583
$1\sigma_u$	−14.0166	−14.0871	−14.1163	−14.1346	−14.2727
$2\sigma_u$	−0.7567	−0.7600	−0.7614	−0.7623	−0.7645
$1\pi_g$ (virtual)	−0.3495	−0.3495	−0.3495	−0.3495	−0.3440
$1\pi_u$	−0.7202	−0.7202	−0.7202	−0.7202	−0.7139

deviation with respect to the LCAO value still being 3.8 eV for $L_{max} = 80$. Inner valence states $2\sigma_g$ and $2\sigma_u$ converge much better, within 0.06 eV of the LCAO values, while outer valence states are described even better by the OCE approach than by LCAO for $L_{max} = 40$.

Summarizing the eigenvalues analysis, it seems that with the evident exception of core states, the valence bound states are described with the same or better accuracy than the LCAO method.

In order to study the convergence in the continuum states, in Table 2 we report the values of cross section (σ) and asymmetry parameter (β) for both states $1\sigma_g$ and $3\sigma_g$ calculated at two photoelectron KEs of 0.03 a.u. and 1 a.u. at increasing L_{max}. We chose these two states in order to discriminate core and outer-valence behaviour, and the two different photoelectron energies to probe convergence both very near and well above the threshold. It is worth noting the very fast convergence of the calculated properties; in particular it is quite surprising that, despite the rather poor description of the core states (slow eigenvalue convergence), their corresponding σ and β values are already converged for small L_{max}. The worst situation (but already much better than the usual experimental uncertainties) is represented by the cross section of the $3\sigma_g$ state near the threshold (KE = 0.03 a.u.). We found that the convergence to the limit of increasing L_{max} is exponential:

$$\sigma(L_{max}) = \sigma_\infty(1 - a e^{-bL_{max}})$$

a and b being constants. This is confirmed by the linear trend of Fig. 1, where we plotted on the Y axis the following quantity:

$$Y(L_{max}) = \log|\sigma_\infty - \sigma(L_{max})|$$

The asymptotic value $\sigma_\infty = 6.095$ Mb has been obtained, requiring the best linear correlation, which in the present case is $r = 99.984\%$. The fast convergence is apparent also if we consider the resonance in the $3\sigma_g$ profiles calculated with both $L_{max} = 80$ and $L_{max} = 40$ and shown in Fig. 2.

A similar convergence analysis for R_{max} can be performed starting from Table 3: σ and β have been obtained by varying R_{max} and keeping fixed $L_{max} = 40$. It is important to observe that the convergence is very fast in all cases well above the threshold (KE = 1 a.u.), while near the threshold a slower behaviour is observed. Moreover, the convergence is not monotonic like for L_{max}, but shows a clear oscillating behaviour. We attributed these deteriorations to the difficulty of reaching the pure Coulomb asymptotic behaviour of the continuum wavefunction. In fact for molecular systems the lower multipoles can give non-negligible contributions to the potential even at rather large distances. In order to

Table 2. Cross section σ (Mb) and asymmetry parameter β of N_2 calculated at a photoelectron KE of 0.03 a.u. and 1 a.u. at different values of L_{max}, R_{max} kept fixed at 10.34 a.u.

Property	L_{max}			
	40	50	60	80
$1\sigma_g$				
KE = 0.03 a.u.				
σ	0.393	0.390	0.389	0.388
β	1.553	1.543	1.538	1.536
KE = 1 a.u.				
σ	0.785	0.780	0.778	0.777
β	1.548	1.548	1.547	1.547
$3\sigma_g$				
KE = 0.03 a.u.				
σ	6.029	6.066	6.083	6.092
β	1.666	1.667	1.667	1.667
KE = 1 a.u.				
σ	2.286	2.288	2.289	2.290
β	1.037	1.031	1.028	1.027

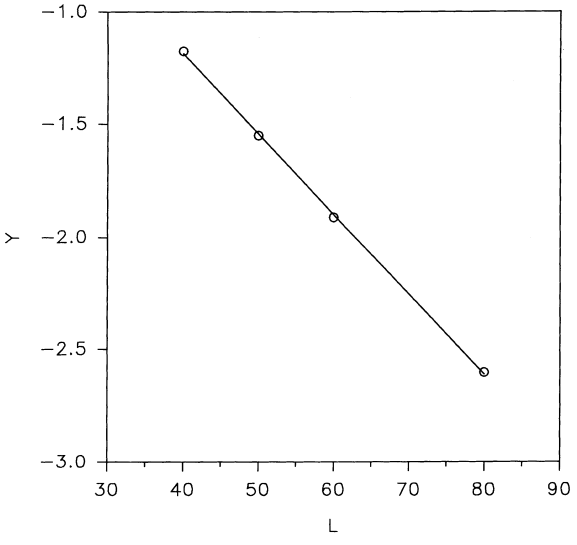

Fig. 1. Convergence of σ ($3\sigma_g$, KE = 0.03 a.u.) with L_{max}. The *circles* are the calculated points; the *straight line* is the linear regression result. See text for details

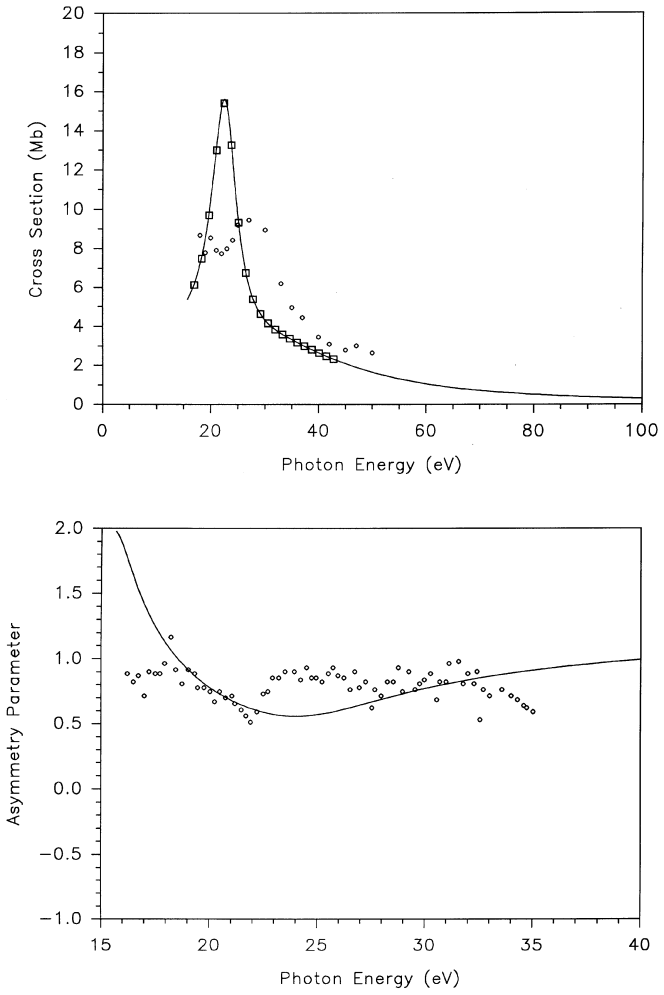

Fig. 2. *Upper panel*: calculated cross section (*solid line*: $L_{max} = 80$; *squares*: $L_{max} = 40$) and experimental data (*circles*) [33] of $3\sigma_g$ ionization in N_2; *lower panel*: calculated asymmetry parameter (*solid line*) and experimental data (*circles*) [34]

investigate better this aspect, we report in Table 4 the values of the various multipole components of the Coulomb potential calculated along the direction of the internuclear axis. The term $L=0$ represents the spherically symmetric contribution and decays as Q/r, where Q is the total charge ($Q=0.5$ due to the TS configuration choice), and the behaviour of the potential can be considered asymptotic when higher multipole contributions ($L > 0$) become negligible with respect to the term with $L=0$. As can be clearly seen, the higher terms are still significant even at $R=31.02$ a.u.; in particular, the quadrupole contribution is only three orders of magnitude lower than the pure asymptotic value. This finding suggests that for molecular systems it is important to compare the continuum wavefunction with a more elaborate asymptotic function which takes into account at least the lowest multipoles. Owing to the availability of recent efficient numerical methods [30–32], this should be a rather straightforward task. It should allow better accuracy and more economical demand since the much shorter R_{max} is needed.

To illustrate the performances of the method, we show in Figs. 2–6 the cross section and the asymmetry parameter profiles presently obtained, all with $L_{max}=80$ and $R_{max}=20.68$ a.u. (otherwise L_{max} is explicitly given), together with the available experimental data for comparison.

In Fig. 2 the ionization from the $3\sigma_g$ orbital is considered: the cross section shows a pronounced shape resonance just above the threshold, followed by a smooth tail. This is in good accordance with experiment [33], although the calculated shape resonance is too sharp and intense. The calculation with $L_{max}=80$ (solid line) is in practice converged; in fact some calculated values obtained with $L_{max}=40$ (squares) are in practice superimposed on the former. On the other hand, the asymmetry parameter profile reproduces nicely the measurements [34]; otherwise the latter are a little scattered. The comparison with available ab-initio static exchange and correlated calculations [16, 35, 36] indicates that while for the asymmetry parameter the results are all in good agreement with each other and with respect to experiment, for the cross section only the present method gives the too sharp and intense resonance. It is worth noting that the present LDA method is not able to describe the interchannel mixing, which gives rise to autoionization resonances and a broadening of the shape resonances. The extension of the present method to the TDLDA formalism [10] will allow the study of such features, as is well known for atoms [37–39], and will be considered in future work for molecular systems in the present OCE framework.

The ionization from the $1\pi_u$ orbital is considered in Fig. 3, here both the cross section and the asymmetry parameter match well the experiments [33, 40] and the previous calculations [16, 35, 36].

In Fig. 4 the results concerning the $2\sigma_u$ ionization are shown. The calculated cross section is qualitatively in good agreement with the experimental one [33], although a global overestimate is present and the structure just above the threshold is absent in the present calculation. In this case the comparison with previous ab initio calculations [16, 35, 36] is very favourable, and this finding suggests that probably the structure found in the experimental profile is very likely a spurious effect of experimental errors. The trend of the asymmetry parameter follows only qualitatively the experiment [34]; the same behaviour is given by the ab initio calculation without interchannel mixing [16], while the introduction of the channel interaction improved the results; therefore we expect that also the TDLDA may improve the present LDA results.

The profiles relative to the inner valence $2\sigma_g$ orbital ionization are given in Fig. 5, together with the experimental data from [41] for the cross section and from [42] for the asymmetry parameter. The calculated cross section is overestimated just above the threshold, while at photon energies higher than 50 eV the agreement is good. At variance, the asymmetry parameter is nicely predicted over the whole energy range reported in the figure.

In Fig. 6 the cross section of the core K shell (N 1*s*) is considered. In the upper panel the N 1*s* partial cross

Table 3. Cross section σ (Mb) and asymmetry parameter β of N_2 calculated at a photoelectron KE of 0.03 a.u. and 1 a.u. at different values of R_{max}; L_{max} kept fixed at a value of 40

Property	R_{max}				
	10.34	15.51	20.68	25.85	31.02
$1\sigma_g$					
KE = 0.03 a.u.					
σ	0.393	0.371	0.374	0.373	0.373
β	1.553	1.530	1.532	1.531	1.532
KE = 1 a.u.					
σ	0.785	0.784	0.784	0.784	0.784
β	1.548	1.548	1.548	1.548	1.548
$3\sigma_g$					
KE = 0.03 a.u.					
σ	6.029	5.687	5.741	5.717	5.734
β	1.666	1.672	1.671	1.671	1.671
KE = 1 a.u.					
σ	2.286	2.299	2.298	2.298	2.299
β	1.037	1.037	1.037	1.037	1.037

Table 4. Values of the lowest multipole components of the Coulomb potential (a.u.) of N_2 calculated along the internuclear axis R (a.u.)

L	R		
	10.34	20.68	31.02
0	4.8×10^{-2}	2.4×10^{-2}	1.6×10^{-2}
2	-3.2×10^{-4}	-4.0×10^{-5}	-1.2×10^{-5}
4	-3.7×10^{-5}	-1.1×10^{-6}	-1.5×10^{-7}
6	-2.6×10^{-6}	-2.0×10^{-8}	-1.1×10^{-9}
8	1.7×10^{-7}	3.2×10^{-10}	8.4×10^{-12}

section is further decomposed into its final symmetry contributions σ and π over a wide photon energy range. In the lower panel the partial final symmetry contributions are compared with the experiments of Shigemasa et al. [43]. The latter has been normalized, matching the π contribution with the present calculation at the photon energy of 445 eV. The agreement of the π final symmetry is excellent; the shape resonance in the σ final symmetry is calculated slightly too sharp and at lower photon energy. Nevertheless, if we consider that off-centre core states are particularly difficult to be treated in an OCE owing to their strong localization, the present results may be considered really encouraging. This finding also suggests that although core states are poorly described in an OCE approach, the cross section is not very sensitive to these kinds of errors, as already observed in the convergence analysis of Table 2. The stability of the cross section of the core N 1*s* ionization is further apparent since it is still possible to extract from the profile even the very weak extended X-ray absorption fine structure (EXAFS) oscillations at large KE, as shown in Fig. 7. The EXAFS signal reported has been obtained as the difference between the calculated cross section and a background obtained by fitting the cross section with a cubic polynomial. A standard backward analysis of our theoretical EXAFS signal [44] gives $R = 2.092$ a.u. for the N-N distance, in good agreement with the actual value employed.

In order to give an idea of the computational performances of the present method, we report the timing

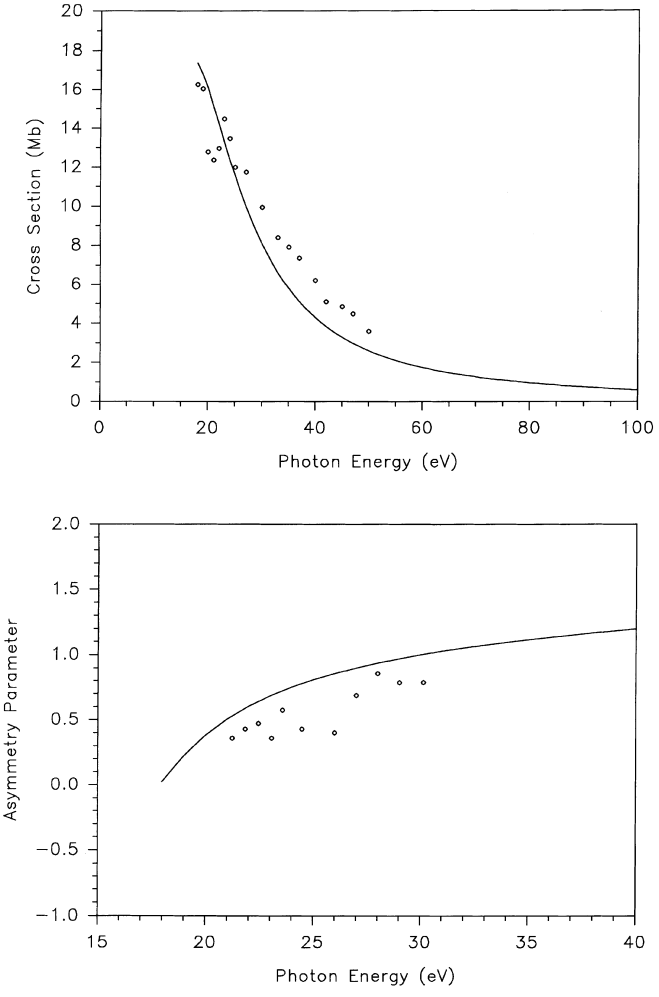

Fig. 3. *Upper panel*: calculated cross section (*solid line*) and experimental data (*circles*) [33] of $1\pi_u$ ionization in N_2; *lower panel*: calculated asymmetry parameter (*solid line*) and experimental data (*circles*) [40]

of the calculations run on a CRAY J916 machine. The main effort of the present method is the inverse iteration process, which is done for each photoelectron energy.

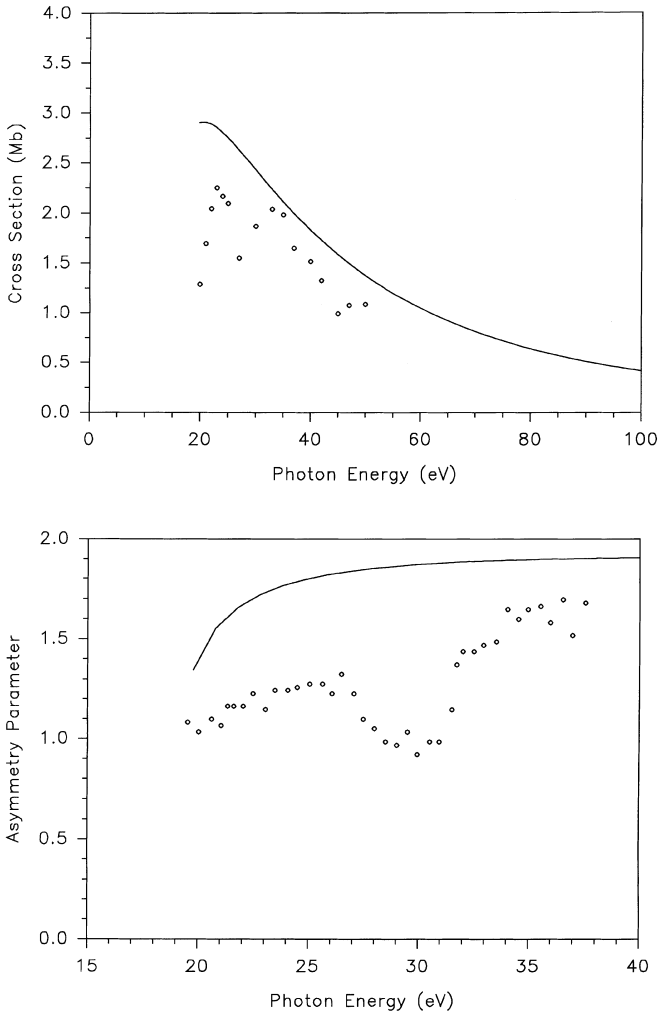

Fig. 4. *Upper panel*: calculated cross section (*solid line*) and experimental data (*circles*) [33] of $2\sigma_u$ ionization in N_2; *lower panel*: calculated asymmetry parameter (*solid line*) and experimental data (*circles*) [34]

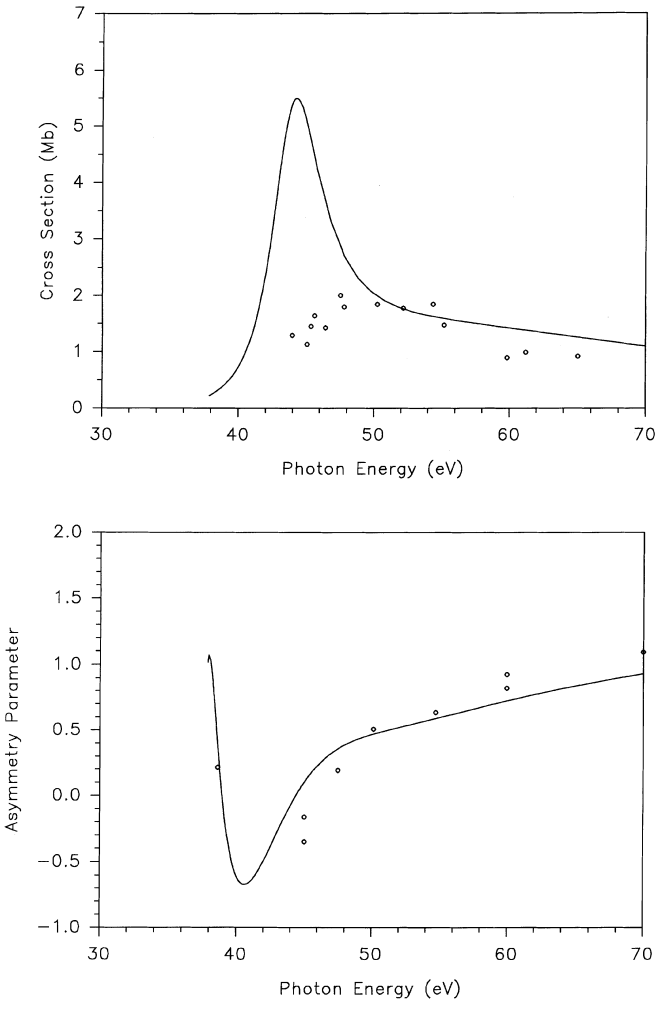

Fig. 5. *Upper panel*: calculated cross section (*solid line*) and experimental data (*circles*) [41] of $2\sigma_g$ ionization in N_2; *lower panel*: calculated asymmetry parameter (*solid line*) and experimental data (*circles*) [42]

However, it is a linear problem so it can be easily parallelized with standard routines up to a factor of 4. In practice, one cross section and asymmetry parameter point needs roughly 30 s to be obtained, and therefore a complete profile of more than 50 points can be obtained in roughly 30 min.

4.2 $(CH_3)_3N$

In order to perform a stringent test of the present method on an extended system, we have chosen the trimethylamine molecule because it has never been theoretically treated with an explicit continuum treatment. Moreover, this is one of the largest molecules for which normalized photoabsorption data are available [45, 46] and therefore a comparison with experiment is possible.

The $(CH_3)_3N$ molecule is an extended system for an OCE approach, so the first step is to check if the present choice in the maximum angular momentum is high enough to ensure accurate results. This can be done by the comparison of the TS Kohn-Sham eigenvalues obtained at the LCAO level with the OCE ones, which are reported in Table 5. Nine orbitals are present in the valence region, and the OCE performs really fairly well for the six highest, with deteriorations with respect to the LCAO method lower than 0.3 eV. In three cases ($6a_1$, 3e and $5a_1$) the OCE performs even better than LCAO, giving lower eigenvalues. The last three inner valence orbitals ($4a_1$, 2e and $3a_1$) are more difficult to be described at the OCE level. This is not surprising since they should be more compact than those in the outer valence, and higher maximum angular momentum would be necessary to gain the same level of accuracy. Nevertheless, the maximum deviation of 2.23 eV is still rather small, if we consider that for N_2 the core N 1*s* state deviates from LCAO by 3.8 eV and gave well converged cross section and asymmetry parameter values. So we can reasonably conclude that the level of accuracy for the present OCE calculation should guarantee reliable results.

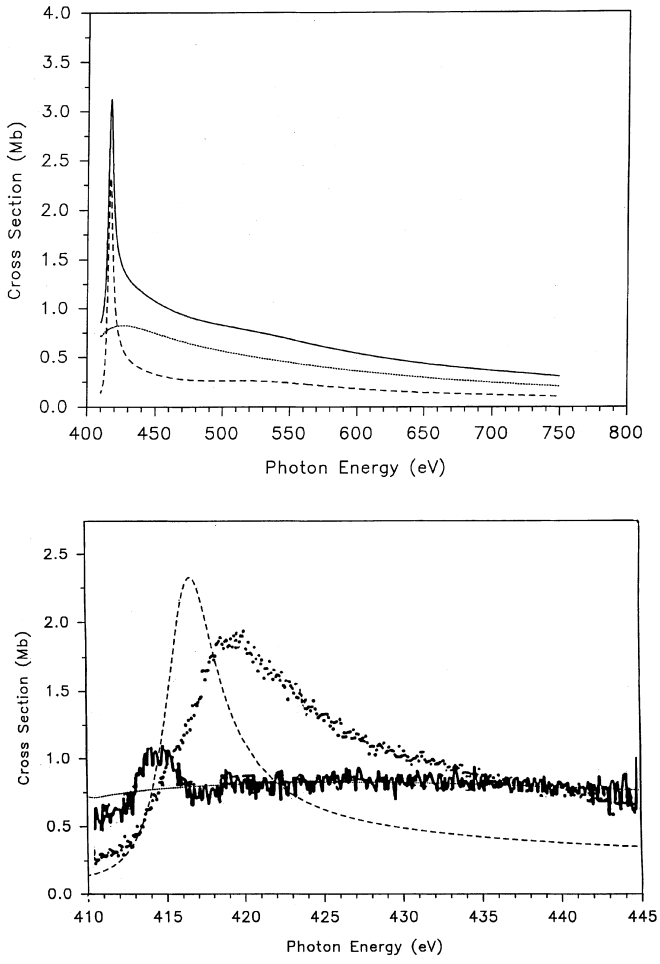

Fig. 6. *Upper panel*: calculated N 1*s* cross section (*solid line*) and its final symmetry contributions (σ: *dashed line*; π: *dotted line*). In the *lower panel* the experimental data of [43] are reported as well: *dots* σ contribution, *solid line* π contribution

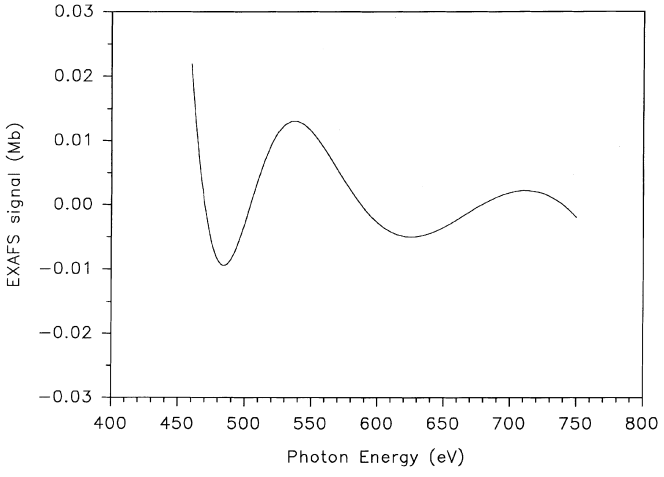

Fig. 7. EXAFS signal extracted from the presently calculated cross section for N_2; see text for details

In Figs. 8 and 9 we have given the calculated cross section and asymmetry parameter relative to the three higher ionizations ($6a_1$, 5e and $1a_2$). The cross section

Table 5. KS eigenvalues of $(CH_3)_3N$ calculated at LCAO and OCE levels, their differences are also reported

Orbital	Eigenvalues (eV)		
	LCAO	OCE	Diff. (eV)
$6a_1$	−8.02	−8.57	−0.55
$5e$	−11.26	−11.10	+0.16
$1a_2$	−11.44	−11.18	+0.26
$4e$	−11.99	−11.95	+0.04
$3e$	−14.15	−14.45	−0.30
$5a_1$	−13.99	−14.37	−0.38
$4a_1$	−16.93	−14.70	+2.23
$2e$	−19.93	−18.10	+1.83
$3a_1$	−26.49	−25.82	+0.67

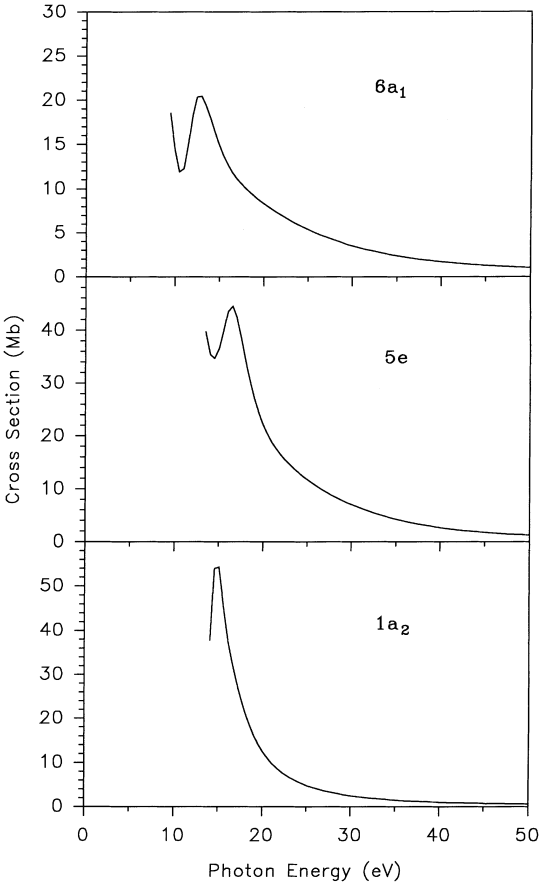

Fig. 8. Calculated cross section profiles for the three outer orbitals in $(CH_3)_3N$

patterns are rather similar: a shape resonance is found in all three cases and the most salient difference is the absolute scale. Thus while the $6a_1$ profile displays the maximum at roughly 20 Mb, the 5e and the $1a_2$ ones are more intense, with maxima respectively at almost 50 Mb and 60 Mb. The asymmetry parameter profiles seem to be more sensitive to the ionization channel, especially in the low KE region, while at higher energy only a small difference in the slope is apparent. Unfortunately, there are no experimental data relative to each orbital partial ionization, so it is not yet possible for a comparison with the actual measurement. On the other hand, the exper-

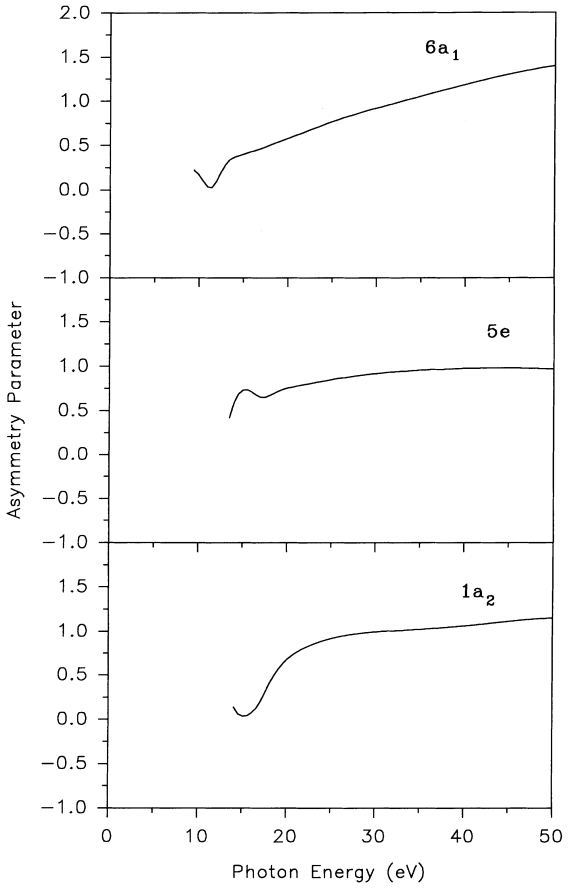

Fig. 9. Calculated asymmetry parameter profiles for the three outer orbitals in $(CH_3)_3N$

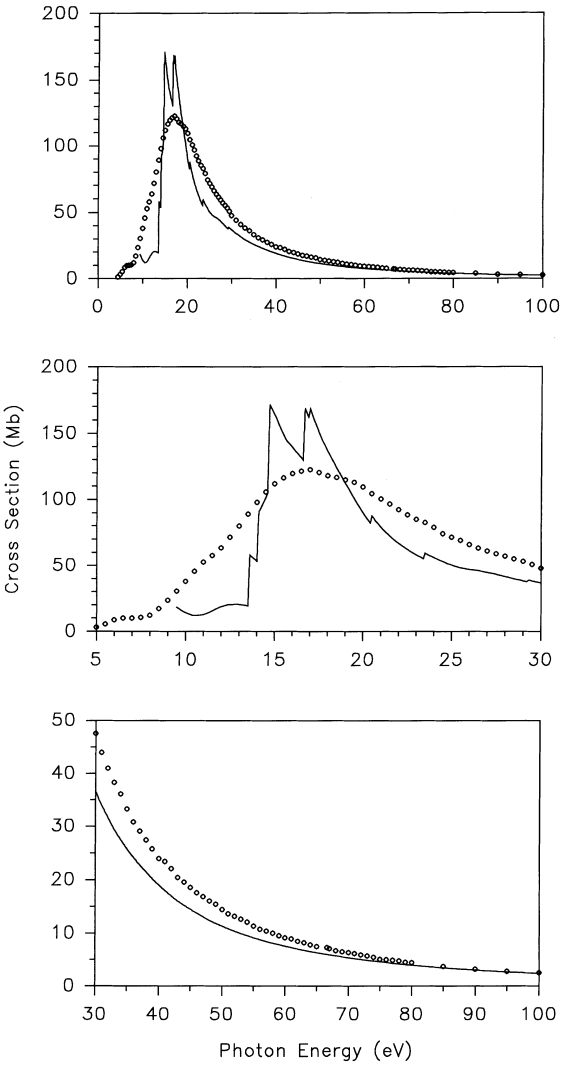

Fig. 10. Calculated total cross section profiles of $(CH_3)_3N$ (*solid line*) and experimental values (*circles*) [46]

imental total photoabsorption profile is available [46], so we have calculated all the partial cross section profiles and summed them in order to obtain the total profile. The calculated and the experimental cross sections are shown in Fig. 10.

Since there are neither experimental nor theoretical data for comparison, we have not reported in the present work the other partial profiles, since we think that a deeper analysis would have been hampered by the lack of significant comparison. Moreover, the calculation of this molecule is justified mainly to demonstrate the capability of the present method to deal with large systems. In any case, we believe that the partial profiles might become interesting if new experimental data will be available or in connection to a systematic study, for example in a series of homologue molecules. Therefore we will consider them in future work, in connection with similar systems, for example $(CH_3)_2NH$ and $(CH_3)NH_2$, for which at least the total photoabsorption measurements are available.

The calculated total cross section profiles of Fig. 10 show many steps in the curve: they are due to the opening of new ionization channels and therefore the cross section increases by a finite quantity in correspondence to the relative ionization threshold. The comparison with experiment (circles in Fig. 10) is favourable: in the upper panel a wide energy range is used and it is apparent that the calculated curve is in good accordance with the experiment, in particular concerning the maximum in the two curves. The central panel reports the energy range just above the threshold: although the global shapes are qualitatively similar, we can observe that while the experimental curve is rather smooth, the calculated profile displays all the steps of the opening channel and its global shape is definitely sharper. In this respect we must keep in mind that the experiment measures the photoabsorption, while the present calculations concern the photoemission. The difference consists in the discrete excitations below each ionization threshold, which should be rather weak since only Rydberg orbitals are expected to contribute as final states [46]. Nevertheless, these effects can smooth the steps in the experiment, masking them with the Rydberg series and making the experimental curve smoother. Moreover, some of the discrepancies between theory and experiment may be due to the too narrow structures predicted by the LDA, as observed for N_2. Finally, the lower panel

shows the high photon energy region where the accord is fairly good.

Although the present analysis has been limited to a few selected points owing to the scarcity of other information sources or analogous calculations, the comparison with experiment can be considered positive and therefore we may say that the present method should be considered for similar analysis of medium sized systems, like molecules or clusters.

The computational effort needed for this molecule is of course much higher than in N_2, owing to the higher extension and the lower symmetry involved. On the same CRAY J916 machine and with a parallelization factor of 4, one cross section point needs 640 s to be obtained, so that a complete profile consisting of 50 points can be obtained within roughly 9 h. Of course, the effort has grown dramatically with respect to N_2, but it is still manageable and even larger or less symmetric systems might be considered for future work.

5 Conclusions

The presently proposed DF-OCE B-splines method for the continuum has been proven to be numerically stable and rather quickly convergent. While very regular convergence has been observed with respect to maximum angular momentum, oscillating behaviour is found with respect to the cut-off radius. A more elaborate asymptotic form of the continuum wavefunction which considers higher multipoles is expected to improve the performance. The observed discrepancies with respect to experiment are probably due to the limitations of the LDA method; the extension to the TDLDA should increase the accuracy. The present method has been applied to the $(CH_3)_3N$ molecule, which is a large system for this kind of calculation. The comparison with available experimental data is good and also the timing scaling properties of the method suggests that it can be profitably used on rather large molecules.

Acknowledgements. This work was supported by grants from MURST (60% and 40% contributions) of Italy and CNR of Rome (Italy).

References

1. Domke M, Remmers G, Kaindl G (1994) Nucl Instr Methods Phys Res Sect B 87:173
2. Dill D, Dehmer JL (1974) J Chem Phys 61:692
3. Langhoff PW (1979) In: Rescigno T, McKoy V, Schneider B (eds) Electron-molecule and photon-molecule collisions. Plenum, New York, p 183
4. Rösch N, Wilhelmy I (1992) Chem Phys Lett 189:499
5. Wilhelmy I, Ackermann L, Görling A, Rösch N (1994) J Chem Phys 100:2808
6. Brosolo M, Decleva P, Lisini A (1994) Chem Phys 181:85
7. Carmona-Novillo E, Moccia R, Spizzo P (1996) Chem Phys 210:435
8. Brosolo M, Decleva P (1992) Chem Phys 159:185
9. Froese Fischer C, Idrees M (1989) Comput Phys 3:53
10. Zangwill A, Soven P (1980) Phys Rev A 21:1561
11. Casida ME (1995) In: Chong DP (ed) Recent advances in density functional methods, part I. World Scientific, Singapore
12. Anderson E, Bai Z, Bishof C, Demmel J, Dongarra J, Du Croz J, Greenbaum A, Hammarling S, McKenney A, Ostrouchov S, Sorensen D (1995) LAPACK user's guide. SIAM, Philadelphia
13. Barnett AR (1982) Comput Phys Commun 27:147
14. Dill D, Dehmer JL (1979) In: Rescigno T, Mckoy V, Schneider B (eds) Electron-molecule and photon-molecule collisions. Plenum, New York, p 225
15. Lane NF (1980) Rev Mod Phys 52:29
16. Cacelli I, Moccia R, Rizzo A (1998) Phys Rev A 57:1895
17. Parr RG, Yang W (1989) Density functional theory of atoms and molecules. Oxford University Press, New York
18. Stener M, Lisini A, Decleva P (1995) Int J Quantum Chem 53:229
19. Leeuwen R van, Baerends EJ (1994) Phys Rev A 49:2421
20. Gisbergen SJA van, Osinga VP, Gritsenko OV, Leeuwen R van, Snijders JG, Baerends EJ (1996) J Chem Phys 105:3142
21. Bishop D (1967) In: Löwdin P-O (ed) Advances in quantum chemistry, vol 3. Academic press, New York
22. Burke PG, Chandra N, Gianturco FA (1972) J Phys B 5:2212
23. Boor C de (1978) a practical guide to splines. Springer, Berlin Heidelberg New York
24. Sapirstein J, Johnson WR (1996) J Phys B At Mol Opt Phys 29:5213
25. Decleva P, Lisini A, Venuti M (1995) Int J Quantum Chem 56:27
26. Baerends EJ, Ellis DE, Ros P (1973) Chem Phys 2:41
27. Vosko SH, Wilk L, Nusair M (1980) Can J Phys 58:1200
28. Sekiya M, Tatewaki H (1987) Theor Chim Acta 71:149
29. Wollrab JE, Laurie VW (1969) J Chem Phys 51:1580
30. Christley JA, Thompson IJ (1994) Comput Phys Commun 79:143
31. Morgan LA (1984) Comput Phys Commun 31:419
32. Noble CJ, Nesbet RK (1984) Comput Phys Commun 33:399
33. Hamnett H, Stoll W, Brion CE (1976) J Electron Spectrosc Relat Phenom 8:367
34. Southworth SH, Parr AC, Hardis JE, Dehmer JL (1986) Phys Rev A 33:1020
35. Veseth L (1994) J Phys B At Mol Opt Phys 27:481
36. Stratmann RE, Bandarage G, Lucchese RR (1995) Phys Rev A 51:3756
37. Stener M, Decleva P, Lisini A (1995) J Phys B At Mol Opt Phys 28:4973
38. Stener M, De Alti G, Decleva P (1997) Chem Phys 222:197
39. Stener M, Decleva P (1997) J Phys B At Mol Opt Phys 30:4481
40. Marr GV, Morton JM, Holmes RM, McKoy DG (1979) J Phys B 12:43
41. Krummacher S, Schmidt V, Wuilleumier F (1980) J Phys B 13:3993
42. Grimm FA, Carlson TA (1983) Chem Phys 80:389
43. Shigemasa E, Ueda K, Sato Y, Sasaki T, Yagishita Y (1992) Phys Rev A 45:2915
44. Filipponi A, Di Cicco A (1995) Phys Rev B 52:15135
45. Olney T, Cann NM, Cooper G, Brion CE (1997) Chem Phys 223:59
46 Burton GR, Chan WF, Cooper G, Brion CE, Kumar A, Meath WJ (1994) Can J Chem 72:529